Supplementary Information

A low iridium content greatly improves the peroxidase-like activity of noble metal nanozymes for sensitive colorimetric detection

Jian Hao,‡ [a] Rui Shang,‡ [a] Miaotian Shi,[a] Jincheng Yuan,[a] Yi Tan,[a] Jiawei Liu*[b] and Kai Cai*[a]*

[a] Life Science Instrumentation Center, College of Chemistry & Environmental Engineering, Yangtze University, Jingzhou 434100, China.

[b] Key Laboratory of Earth and Planetary Physics, Institute of Geology and Geophysics, Innovation Academy for Earth Sciences, Chinese Academy of Sciences, Beijing 100029, China.

*Corresponding Author.

E-mail: shimiaotian@yangtzeu.edu.cn (M. S.); caikai2000@163.com (K. C.); liujiawei@mail.iggcas.ac.cn (J. L.)

Materials

Tellurium dioxide powder (TeO_2, 99.99%), and selenous acid (H_2SeO_3, 99.99%) were purchased from Aladdin Chemistry Co., Ltd. Hydrazine monohydrate ($N_2H_4\,H_2O$, 85%, AR), sodium dodecyl sulfate (SDS, 99%), Chloroplatinic acid ($H_2PtCl_6\ 6H_2O$, AR), Tetrachioroauric(III) acid tetrahydrate($HAuCl_4\ 4H_2O$, AR), Iridic chloride ($IrCl_4$, AR), polyvinylpyr-rolidone (PVP10 Average molecular weight 58000 AR), hydrogenperoxide (H_2O_2, 30%, AR) were provided by Sinopharm Chemical Reagent Co., Ltd. 3,3',5,5'-tetramethylbenzidine (TMB), o-Phenylenediamine ($C_6H_8N_2$, OPD, 98%), Citric acid/sodium was obtained from McLean chemical reagent Co., Ltd.

Material Characterization

Transmission electron microscopy (TEM) imaging was conducted on a FEI TECNAI F30 microscope operated at 200 kV and copper grids were used to load the samples. All values of the material sizes were measured through TEM images. X-ray spectroscopy (EDS) was carried out under the high-angle annular dark field (HAADF) mode with an EDAX attachment. Inductively coupled plasma-mass spectrometry (ICP-MS) measurements were performed on NexION 300Q (PerkinElmer, USA). X-ray diffraction (XRD) was tested on a Bruker D8 Advance X-ray diffractometer with Cu Kα radiation. Samples were prepared by depositing nanostructures on glass. The scanning speed was set as 15 degrees/min. X-ray photoelectron spectra (XPS) were collected on an ESCALAB 250Xi spectrophotometer (Thermo Fisher) with Al Kα X-ray radiation and calibrated using the C 1s peak (284.8 eV). UV-vis-NIR absorption spectra were measured by a Lambda 750UV-Vis-NIR spectrophoto meter (PerkinElmer, USA).

Measurement of the specific activity

Specific activity (SA) was measured according to the protocol reported in former reports.[1] Specifically, at 20 ℃, 0.1 M citric acid/sodium citrate was selected as buffer (pH=4.0). H_2O_2, nanozyme material, TMB (50 μL 10 mg/mL) were added successively. The final volume is controlled at 1 mL, in which the concentration of H_2O_2 is 1.0 M,

and the quality of nanozyme material added each time is controlled. The absorbance of the reaction solution at λ_{max} = 653 nm was measured by UV-vis spectrophotometer at the interval of 1 second immediately after the addition of all substances for 50 s. The absorbance-time curve is then obtained and SA is calculated by the following equation.

$$b_{nanozyme} = \frac{V}{\varepsilon l} X \frac{\Delta A}{\Delta t}$$

where $b_{nanozyme}$ is the nanozyme activity (U), V is the total volume of reaction solution (μL), ε is the molar absorption coefficient of the TMB substrate (39,000 M^{-1} cm^{-1} at 653 nm), l is the optical path length through reaction solution (cm), and ΔA/Δt is the initial rate of the absorbance change (min^{-1}). When using different amounts of the nanozyme to measure the peroxidase-like activity, the specific activity of the nanozyme was determined using the following equation:

$$SA = \frac{b_{nanozyme}}{m}$$

where SA is the specific activity of the nanozyme (U mg^{-1}), and m is the nanozyme amount (mg).

Kinetic analysis

Peroxidase-like activities of the nanozyme material were evaluated by the steady-state kinetic assays, according to the previous report.[2] Specifically, 0.1 M citric acid/sodium citrate were added successively as buffer (pH=4.0). H_2O_2, nanozyme material (50 μL, 1 mg/L) and TMB were added in the cuvette (path length, l=1.0 cm) at 20 ℃. The final volume is controlled at 1 mL, in which the concentration of H_2O_2 is 2.0 M, and TMB is controlled as the variable. After adding all substances, the absorbance of the reaction solution at λ_{max} = 653 nm was measured by UV-vis spectrophotometer at an interval of 2 seconds for 50 s. Then, the absorbance and time curve is obtained, from which the initial reaction rate is calculated and the maximum reaction rate V_{max} and the Michaelis constant (K_m) are accessed by the Michaelis-Menten equation.

$$V = \frac{V_{max}[S]}{K_m + [S]}$$

where V_{max} is the maximal reaction velocity, [S] is the concentration of TMB, and K_m is the Michaelis constant. The values of K_m and V_{max} can be obtained from the double reciprocal plots.

Stability test process

Citric acid/sodium citrate (0.1 M) was selected as buffer (pH=4.0) at 25 ℃. TMB (50 μL, 10 mg/mL), nanozyme material (50 μL, 0.5 mg/L) and H_2O_2 (30%) were added successively. The final volume is controlled at 1 mL. The absorbance of the reaction solution at λ_{max}=653 nm was recorded by UV-vis spectrophotometer after the addition of all substances for 50 s. The same procedure was used every day for ten days.

Measurement of absorption spectrum of reaction system

50 μL TMB (10 mg/mL), 50 μL nanozyme material (0.5 mg/L) and 100 μL H_2O_2 (30%) were added into a tube containing 800 μL citric acid/sodium citrate buffer solution (0.1 M, pH=4.0) at 25 ℃. The absorption spectra were recorded in the range of 300 ~ 800 nm after incubation for 1 min.

Measurement of absorbance of reaction system

When measuring absorbance over time, 50 μL TMB (10 mg/mL), 50 μL nanozyme material (0.5 mg/L) and 100 μL H_2O_2 (30%) were added into a 2 mL tube containing 800 μL citric acid/sodium citrate buffer solution (0.1 M, pH=4.0) at 25 ℃. After incubation for 1 min, the absorbance of the solution at 653 nm was measured by UV-vis spectrophotometer at an interval of 2 seconds for 50 s. When measuring absorbance at different pH, the citric acid/sodium citrate buffer solution (0.1 M, pH=2.0, 3.0, 4.0, 5.0, 6.0 or 7.0) was used. When measuring absorbance at different temperature, the solution temperature was controlled at 10, 20, 30, 40, 50 or 60 ℃.

Isopropanol quenching hydroxyl radical test process

In simple terms, 50 μL isopropanol, 50 μL TMB (10 mg/mL), 50 μL H_2O_2 with different concentrations and 50 μL nanozyme solution (1 mg/L) were added to sodium citrate (0.1 M, pH=4.0). The final volume is controlled at 1 mL, After adding all substances, the absorbance of the reaction solution at λ_{max} = 653 nm was measured by

UV-vis spectrophotometer at an interval of 1 seconds for 50 s.

Colorimetric detection of OPD

The detection of OPD was conducted as follows: 100 μL PtAuIr nanozyme solution (10 mg/L) and 100μL H_2O_2 (30%) were added into a 2 mL tube containing 700 μL citric acid/sodium citrate buffer solution (0.1 M, pH=4.0). Then, 100 μL OPD solutions of different concentrations were added to the obtained mixture and incubated at room temperature for 5 min. The absorption spectra were recorded in the range of 300 ~ 600 nm. All measurements were performed in triplicate, and the standard deviation was plotted as error bars.

Theoretical calculations.

The Vienna Ab Initio Package (VASP) was employed to perform all the density functional theory (DFT) calculations within the generalized gradient approximation (GGA) using the Perdew, Burke, and Enzerhof (PBE) formulation.[3-5] The projected augmented wave (PAW) potentials were applied to describe the ionic cores and take valence electrons into account using a plane wave basis set with a kinetic energy cutoff of 500 eV.[6,7] Partial occupancies of the Kohn–Sham orbitals were allowed using the Gaussian smearing method and a width of 0.05 eV. The electronic energy was considered self-consistent when the energy change was smaller than 10^{-5} eV. A geometry optimization was considered convergent when the force change was smaller than 0.05 eV/Å. Grimme's DFT-D3 methodology was used to describe the dispersion interactions.[8] The vacuum spacing perpendicular to the plane of the structure is 20 Å. The Brillouin zone integral utilized the surfaces structures of 2×2×1 monkhorst pack K-point sampling. Finally, the adsorption energies(E_{ads}) were calculated as $E_{ads}= E_{ad/sub} - E_{ad} - E_{sub}$, where $E_{ad/sub}$, E_{ad}, and E_{sub} are the total energies of the optimized adsorbate/substrate system, the adsorbate in the structure, and the clean substrate, respectively. The free energy was calculated using the equation:

$$G=E_{ads}+ZPE-TS$$

where G, E_{ads}, ZPE and TS are the free energy, total energy from DFT calculations, zero point energy and entropic contributions, respectively.

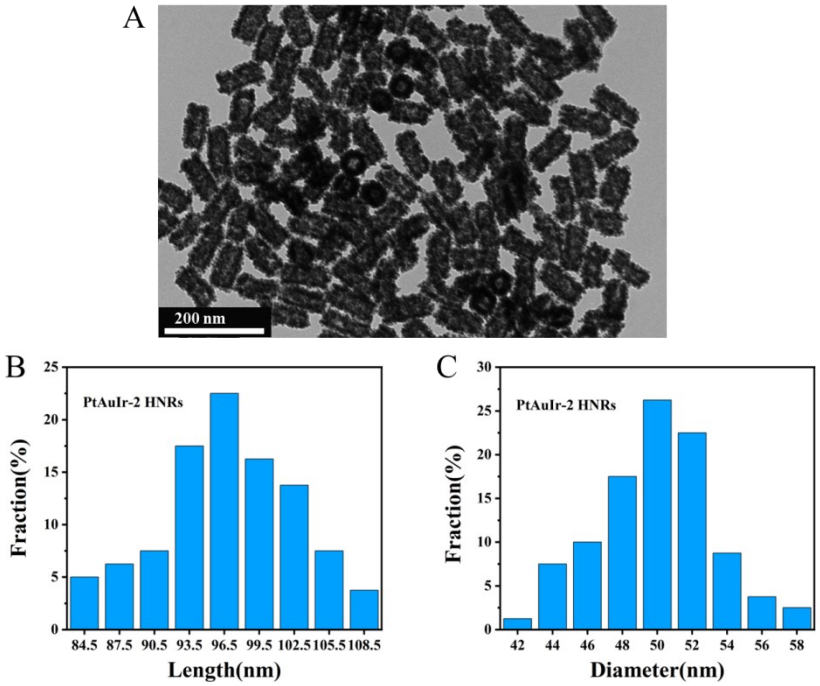

Figure S1 (A) TEM of PtAuIr-2 HNRs. Statistical value of diameter (B) and length (C) of PtAuIr-2 HNRs.

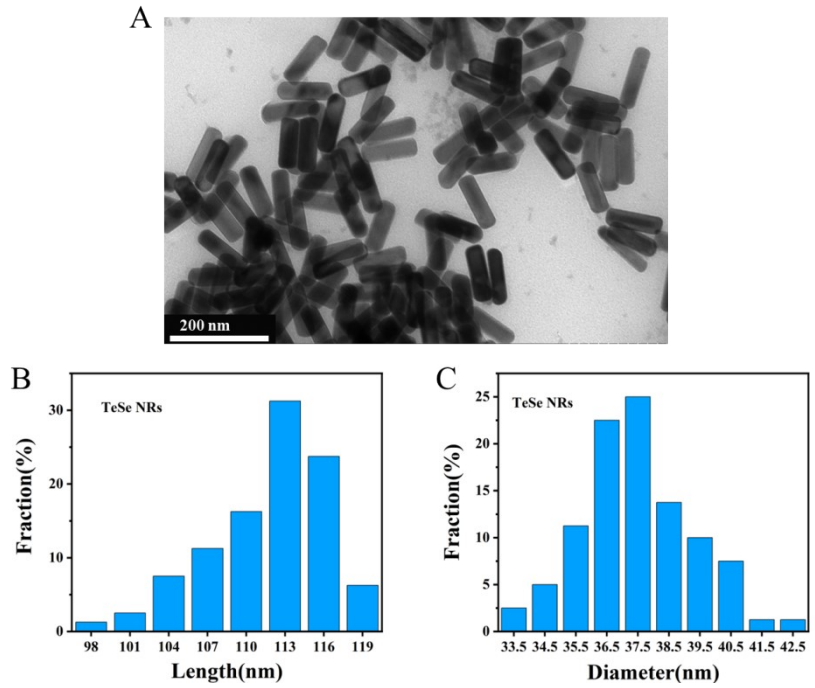

Figure S2 (A) TEM of TeSe nanorod. Statistical value of diameter (B) and length (C) of TeSe nanorods.

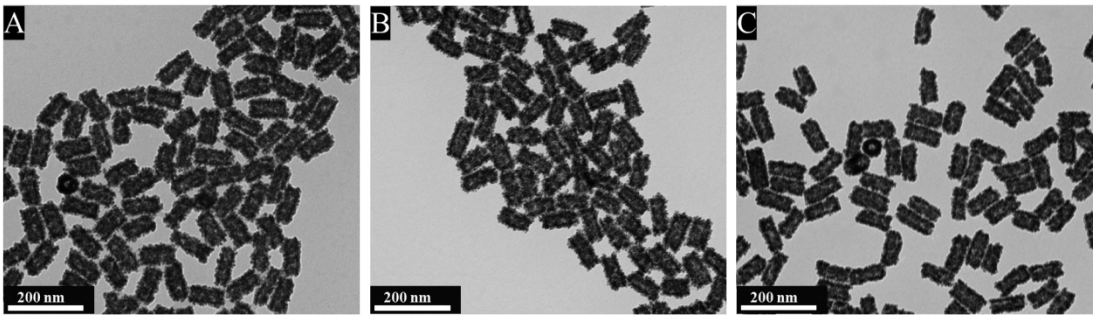

Figure S3 TEM of PtAu HNRs, PtAuIr-1 HNRs and PtAuIr-3 HNRs.

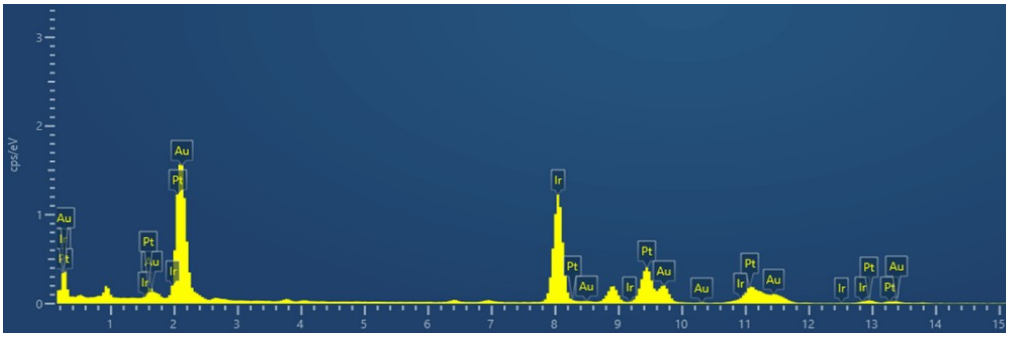

Figure S4 EDS of PtAuIr-2 HNRs.

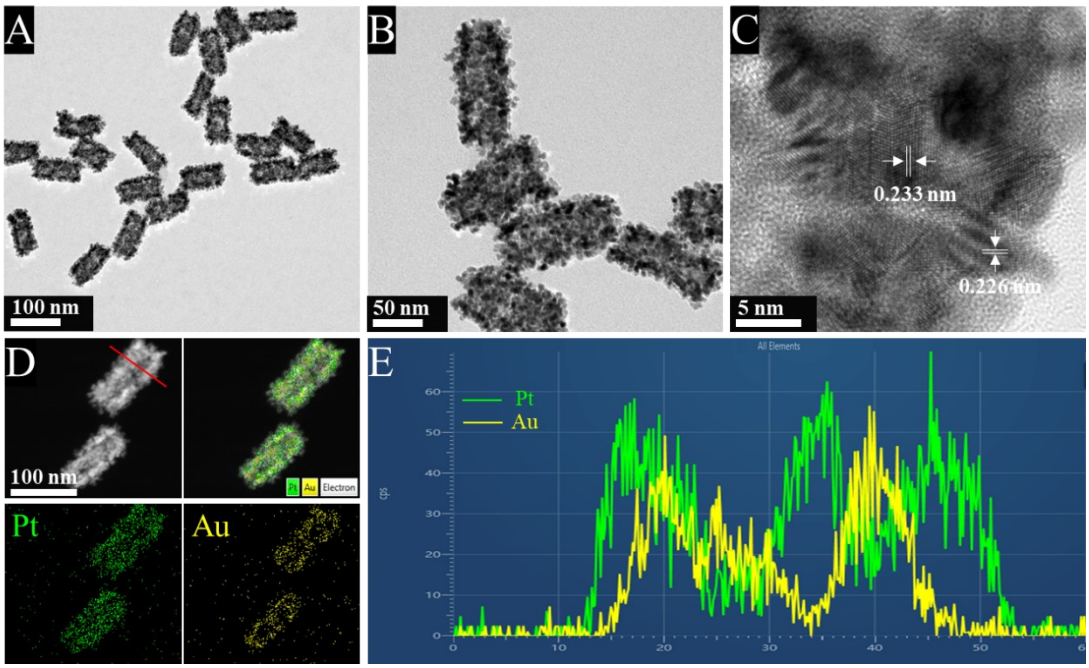

Figure S5 (A,B) TEM images, (C) HRTEM image, (D) HAADF-STEM image and EDS mapping images of PtAu HNRs. (E) EDS line scanning of the PtAu HNRs.

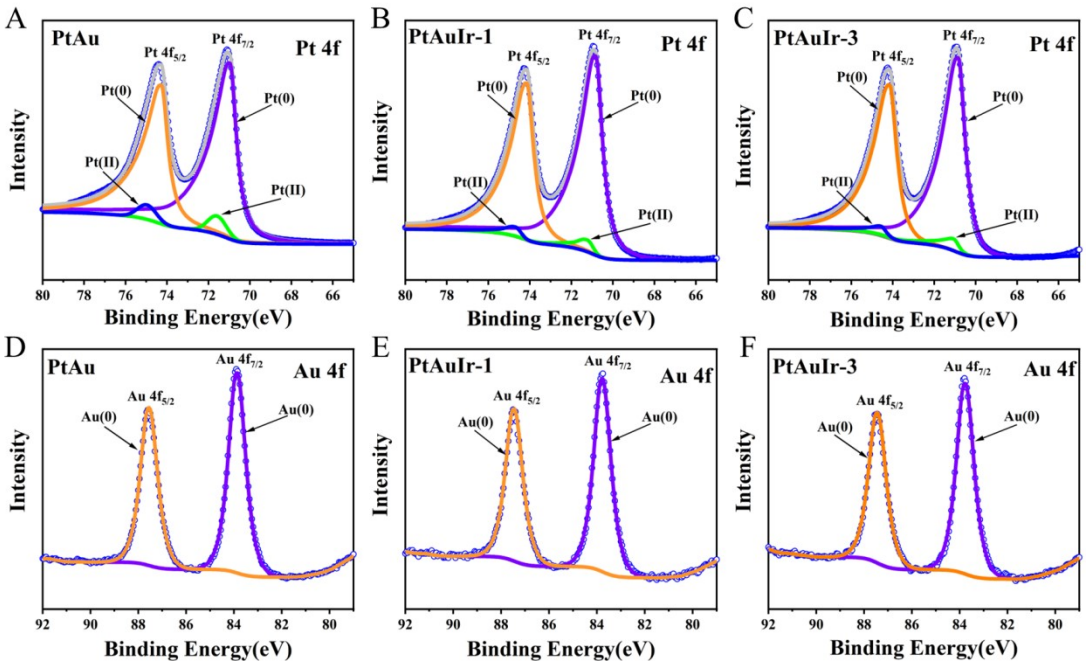

Figure S6 XPS spectra of Pt 4f for PtAu (A), PtAuIr-1 (B), PtAuIr-3 (C); Au 4f for PtAu (D) PtAuIr-1 (E), PtAuIr-3 (F).

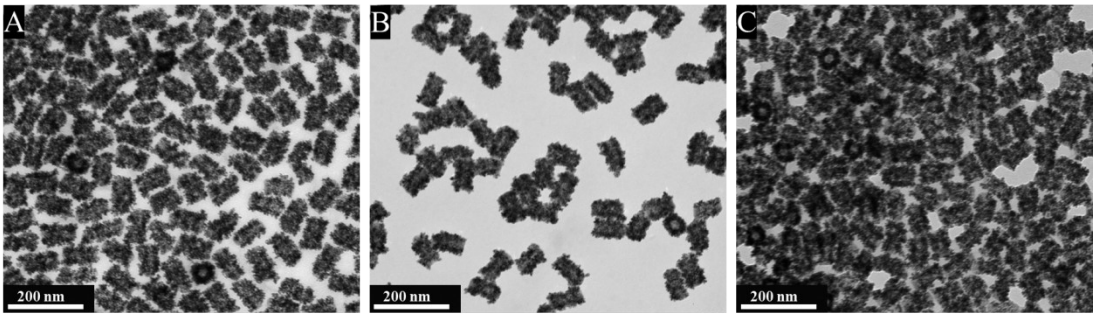

Figure S7 TEM of Pt HNRs, PtIr-1 HNRs and PtIr-2 HNRs.

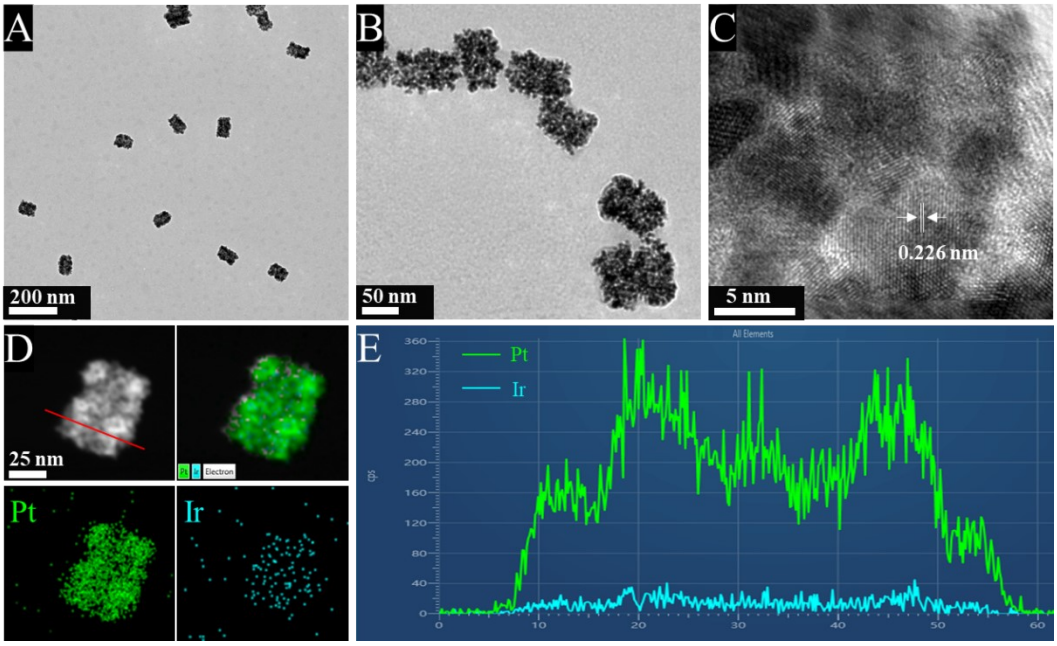

Figure S8 (A, B) TEM images, (C) HRTEM image, (D) HAADF-STEM image and EDS mapping images of PtIr HNRs. (E) EDS line scanning of the PtIr HNRs.

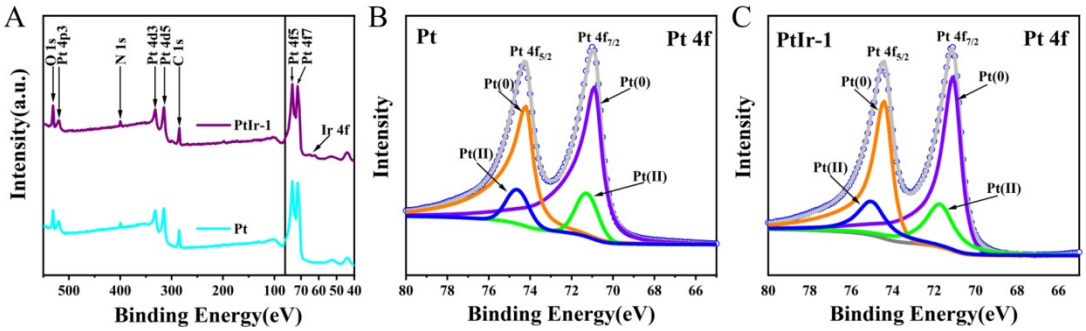

Figure S9 (A) Wide XPS spectrum. XPS spectra of Pt 4f for Pt (B) PtIr-1(C).

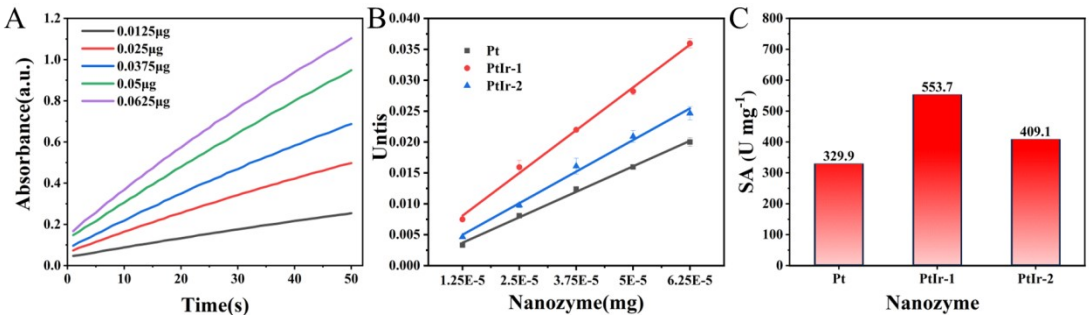

Figure S10 (A) Time-absorbance curves under different mass of PtIr-1 nanozyme. (B) Measurement of SA values of Pt, PtIr-1, PtIr-2 nanozyme. (C) The SA of different nanozyme.

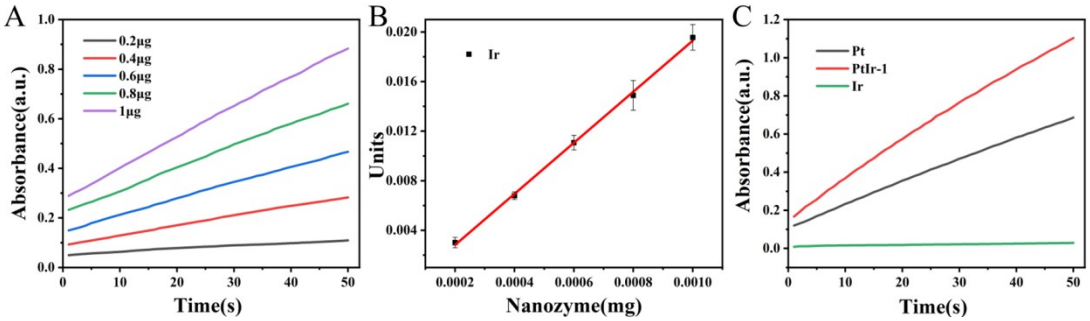

Figure S11 (A) Time-absorbance curves under different mass of Ir nanozymes. (B) Measurement of SA values of Ir nanozyme. (C) Time-absorbance curves of different nanozymes with the same mass (0.0625 μg).

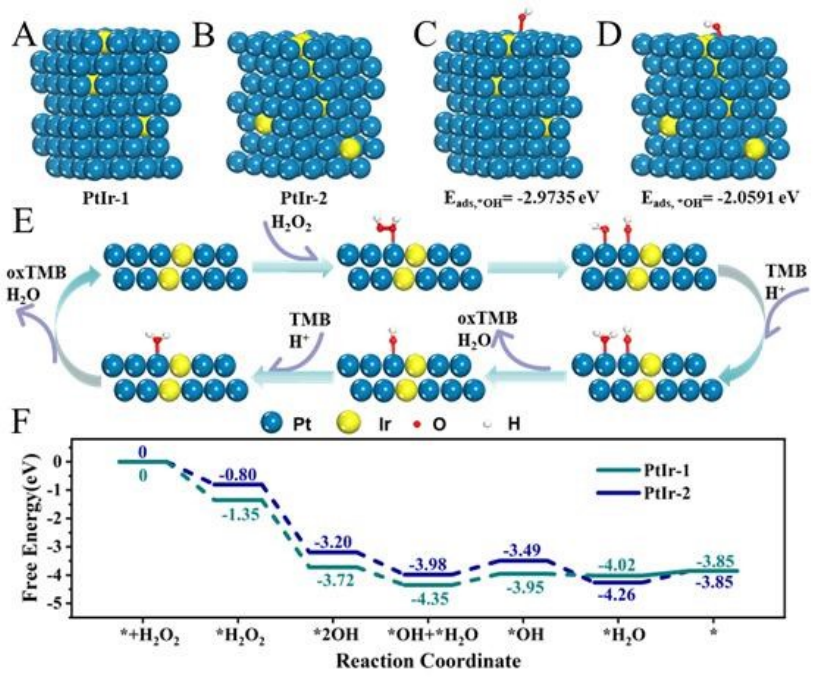

Figure S12 (A) Structure of the PtIr-1 nanozyme. (B) Structure of the PtIr-2 nanozyme. (C) The adsorption energy of hydroxyl radicals on PtIr-1(111). (D) The adsorption energy of hydroxyl radicals on PtIr-2(111). (E) Reaction diagram of the catalytic process. (F) Energy change diagram of the reaction on two PtIr HNRs.

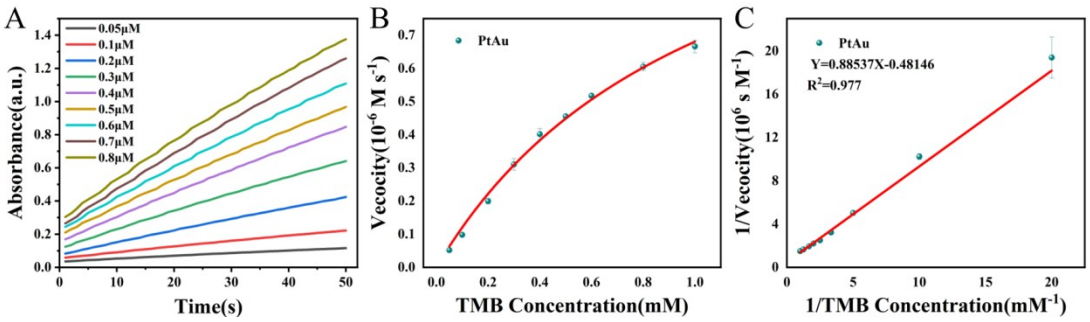

Figure S13 (A) Time-absorbance curves at different TMB concentrations of PtAu nanozyme. (B) Initial reaction velocity against TMB concentration of PtAu nanozyme. (C) Double-reciprocal plots for PtAu nanozyme.

Table S1 The elements ratio of all HNRs.

Samples	Pt (μg/L)	Au (μg/L)	Ir (μg/L)
PtAu	170.8028	70.2986	/
PtAuIr-1	142.3450	53.7938	2.3484
PtAuIr-2	139.1440	63.2967	6.9864
PtAuIr-3	113.7989	50.5932	8.0784
PtAuIr-4	129.5195	52.1276	13.9100
Pt	148.4923	/	/
PtIr-1	173.4708	/	4.9584
PtIr-2	155.8484	/	10.4296

Table S2 The specific activities of nanozymes.

	Substrate	SA(U mg^{-1})	Ref.
HG-Heme	TMB	67.3	9
FeNCP/NW	TMB	86.9	10
PdPtAu alloy	TMB	81.245	11
A-Ru	TMB	164.46	12
Os NPS	TMB	393	13
USPBNPS	TMB	465.8	14
FeN_3P	TMB	316	15
Natural HRP	TMB	327	16
H-Pt_3Sn	TMB	345.32	17
FeSA-PtC	TMB	87.7	18
PtPdAu HNRs	TMB	563.71	1
PtAuIr-2	TMB	863.2	
PtAuIr-3	TMB	666.9	
PtAuIr-1	TMB	638.6	
PtAuIr-4	TMB	546.6	This
PtAu	TMB	508.2	work
PtIr-1	TMB	553.7	
PtIr-2	TMB	409.1	
Pt	TMB	329.9	

Table S3 Comparison of limit of detection of OPD using different nanozymes.

Method	Materials	Linear Range (μM)	LOD (μM)	Ref.
Colorimetry	Fe_3O_4/N-GQDs	1-90	0.23	19
Colorimetry	Tar-IrNPs	4.6-46	0.17	20
Colorimetry	N,Cu-CDs	5-200	1.12	21
Colorimetry	AgNPs	1-80	0.161	22
Colorimetry	SW-Fe_2O_3/MnO_2	16.7-500	5	23
Colorimetry	PtAuIr NRs	0.5-100	0.076	This work

References

1 Y. Tan, J. Yuan, R. Shang, J. Hao, S. Hu and K. Cai, *Dalton Trans.*, 2024, **53**, 5624-5631.

2 Z. Xi, K. Wei, Q. Wang, M. J. Kim, S. Sun, V. Fung and X. Xia, *J. Am. Chem. Soc.*, 2021, **143**, 2660-2664.

3 G. Kresse and J. Furthmüller, *Phys. Rev. B*, 1996, **54**, 11169-11186.

4 J. P. Perdew, K. Burke and M. Ernzerhof, *Phys. Rev. Lett.*, 1996, **77**, 3865-3868.

5 G. Kresse and D. Joubert, *Phys. Rev. B*, 1999, **59**, 1758-1775.

6 P. E. Blöchl, *Phys. Rev. B,* 1994, **50**, 17953-17979.

7 S. Grimme, J. Antony, S. Ehrlich and H. Krieg, *J. Chem. Phys.*, 2010, **132**, 154104.

8 G. Henkelman, B. P. Uberuaga and H. Jónsson, *J. Chem. Phys.*, 2000, **113**, 9901-9904.

9 W. Xu, W Song, Y Kang, L. Jiao, Y. Wu, Y. Chen, X. Cai, L. Zheng, W. Gu and C. Zhu, *Anal. Chem.*, 2021, **93**, 12758-12766.

10 S. Ding, J. A. Barr, Z. Lyu, F. Zhang, M. Wang, P. Tieu, X. Li, M. H. Engelhard, Z. Feng, S. P. Beckman, X. Pan, J. Li, D. Du and Y Lin, *Adv. Mater.*, 2023, 2209633.

11 L. Huang, Y. Zhou, Y. Zhu, H. Su, S. Yang, L. Feng, L. Zhao, S. Liu and K. Qian, *Biosens. Bioelectron.*, 2022, **210**, 114254.

12 Y. Tang, Y. Wu, W. Xu, L. Jiao, Y. Chen, M. Sha, H. Ye, W. Gu and C. Zhu, *Anal. Chem.*, 2021, **94**, 1022-1028.

13 S. He, L. Yang, P. Balasubramanian, S. Li, H. Peng, Y. Kuang, H. Deng and W. Chen, *J. Mater. Chem. A*, 2020, **8**, 25226-25234.

14 Z. Qin, B. Chen, Y. Mao, C. Shi, Y. Li, X. Huang, F. Yang and N. Gu, *ACS Appl. Mater. Interfaces*, 2020, **12**, 57382-57390.

15 S. Ji, B. Jiang, H. Hao, Y. Chen, J. Dong, Y. Mao, Z. Zhang, R. Gao, W. Chen, R. Zhang, Q. Liang, H. Li, S. Liu, Y. Wang, Q. Zhang, L. Gu, D. Duan, M. Liang, D. Wang, X. Yan and Y. Li, *Nat. Catal.*, 2021, **4**, 407-417.

16 X. Niu, Q. Shi, W. Zhu, D. Liu, H. Tian, S. Fu, N. Cheng, S. Li, J. N. Smith, D. Du and Y. Lin, *Biosens. Bioelectron.*, 2019, **142**, 111495.

17 Y. Tang, Y. Chen, Y. Wu, W. Xu, Z. Luo, H. Ye, W. Gu, W. Song, S. Guo, and C. Zhu, *Nano Lett.*, 2022, **23**, 267-275.

18 Y. Chen, L. Jiao, H. Yan, W. Xu, Y. Wu, L. Zheng, W. Gu and C. Zhu, *Anal. Chem.*, 2021, **93**, 12353-12359.

19 B. Shi, Y. Su, L. Zhang, M. Huang, X. Li and S. Zhao, *Nanoscale*, 2016, **8**, 10814-10822.

20 S. Hao, C. Fu, L. Zhou, Z. Guo and Q. Song, *J. Mater, Chem. B*, 2023, **11**, 2770-2777.

21 L. Lin, Y. Xiao, Y. Wang, Y. Zeng, Z. Lin and X. Chen, *Microchim. Acta*, 2019, **186**, 1-8.

22 N. Li, Y. Gu, M. Gao, Z. Wang, D. Xiao, Y. Li, R. Lin and H. He, *Spectrochim. Acta, Part A*, 2015, **140**, 328-333.

23 R. María-Hormigos, B. Jurado-Sánchez and A. Escarpa, *Anal. Chem.*, 2018, **90**, 9830-9837.